Follistatin is critical for mouse uterine receptivity and decidualization

Paul T. Fullerton Jr.[a,b,c,d], Diana Monsivais[a,c,d], Ramakrishna Kommagani[e], and Martin M. Matzuk[a,b,c,d,e,f,1]

[a]Department of Pathology and Immunology, Baylor College of Medicine, Houston, TX 77030; [b]Department of Molecular and Human Genetics, Baylor College of Medicine, Houston, TX 77030; [c]Center for Reproductive Medicine, Baylor College of Medicine, Houston, TX 77030; [d]Center for Drug Discovery, Baylor College of Medicine, Houston, TX 77030; [e]Department of Molecular and Cellular Biology, Baylor College of Medicine, Houston, TX 77030; and [f]Department of Pharmacology, Baylor College of Medicine, Houston, TX 77030

Contributed by Martin M. Matzuk, April 26, 2017 (sent for review December 19, 2016; reviewed by Kate L. Loveland and Felice Petraglia)

Embryo implantation remains a significant challenge for assisted reproductive technology, with implantation failure occurring in ∼50% of in vitro fertilization attempts. Understanding the molecular mechanisms underlying uterine receptivity will enable the development of new interventions and biomarkers. TGFβ family signaling in the uterus is critical for establishing and maintaining pregnancy. Follistatin (FST) regulates TGFβ family signaling by selectively binding TGFβ family ligands and sequestering them. In humans, FST is up-regulated in the decidua during early pregnancy, and women with recurrent miscarriage have lower endometrial expression of FST during the luteal phase. Because global knockout of *Fst* is perinatal lethal in mice, we generated a conditional knockout (cKO) of *Fst* in the uterus using progesterone receptor-cre to study the roles of uterine *Fst* during pregnancy. Uterine *Fst*-cKO mice demonstrate severe fertility defects and deliver only 2% of the number of pups delivered by control females. In *Fst*-cKO mice, the uterine luminal epithelium does not respond properly to estrogen and progesterone signals and remains unreceptive to embryo attachment by continuing to proliferate and failing to differentiate. The uterine stroma of *Fst*-cKO mice also responds poorly to artificial decidualization, with lower levels of proliferation and differentiation. In the absence of uterine FST, activin B expression and signaling are up-regulated, and bone morphogenetic protein (BMP) signals are impaired. Our findings support a model in which repression of activin signaling by FST enables uterine receptivity by preserving critical BMP signaling.

female infertility | implantation failure | TGFβ signaling | activin antagonism

Mouse models are powerful tools for improving our understanding of uterine receptivity because mice can be easily manipulated with well-established genetic tools and experimental approaches (1). Studies using mice have shown that TGFβ family growth factors play critical roles in establishing uterine receptivity. The TGFβ family operates through a shared mechanism. The signaling cascade is initiated by binding of homodimeric or heterodimeric ligands to a cell-surface receptor complex composed of a type 2 receptor kinase and its partner type 1 receptor kinase. Once the ligand binds, the type 2 receptor phosphorylates and activates the type 1 receptor. The activated type 1 receptor kinase phosphorylates receptor SMADs, enabling them to form a complex with the co-SMAD, SMAD4. The resulting heterotrimeric SMAD complex concentrates in the nucleus where it regulates gene expression in conjunction with of a multitude of cofactors. Uterine conditional knockout (cKO) of TGFβ superfamily growth factors bone morphogenetic protein 2 (BMP2), type 1 receptors ALK2 and ALK3, and type 2 receptor bone morphogenetic protein receptor 2 (BMPR2) in mice have shown that local uterine TGFβ family signaling plays key roles in regulating embryo attachment and invasion as well as endometrial stromal cell decidualization (2–5).

Follistatin (FST) is a regulator of TGFβ family signaling and acts by selectively binding to TGFβ family ligands and preventing ligand binding to the receptor complex (6–8). There are two major isoforms of FST, FST288, which is anchored to the cell surface by interactions with heparin sulfate proteoglycans (9), and FST315, which is the predominant form found in circulation. In humans, aberrant expression of FST and activins are implicated in infertility; dysregulation of FST, activins, and inhibins was reported in women with impending abortion (10), recurrent miscarriage (11, 12), hypertensive disorders during pregnancy (13), and repeated implantation failure after in vitro fertilization (14). However, the role that FST plays in normal pregnancy remains uncertain.

FST knockout is perinatal lethal in mice (15), precluding study of its role in reproduction with a global inactivation. Several studies have sought to overcome limitations of the global knockout and define the roles of FST in female reproduction. Systemic FST overexpression causes female infertility resulting from blockages in ovarian folliculogenesis and abnormal uterine development, resulting in thin uteri (16). The role of FST in the ovary was further characterized by conditional ablation of *Fst* in the granulosa cells of the ovary using anti-Müllerian hormone receptor type 2-cre (17). These ovarian cKO mice were subfertile because of ovarian developmental defects that progressed into premature ovarian failure and sterility later in life (17). Three recent studies have taken yet another approach, generating mice that express only one of the two major isoforms, FST288 or FST315, driven by either native human or murine promoter sequences (18–20). All three studies reported female infertility, primarily resulting from the critical role that FST has been shown to play in ovarian function (17); however, the roles that FST plays in the uterus are unclear from these studies. To address the roles of uterine FST during pregnancy, we generated a conditional knockout of *Fst* in the uterus of adult female mice using progesterone receptor-cre (*Pgr-cre*). Uterine deletion of *Fst* precluded uterine receptivity to embryo attachment and compromised decidualization.

Significance

An estimated 50% of in vitro fertilization attempts fail to achieve implantation, making implantation one of the most significant challenges in the assisted reproductive technologies (ART) clinic. Unfortunately, no effective treatments or biomarkers are available for the receptivity of the uterus to embryo implantation. Understanding the molecular mechanisms underlying implantation will enable future advances in ART to improve success rates and reduce the emotional, physical, and financial toll that ART failure takes on patients. We generated conditional knockout of follistatin in the uterus and demonstrated that follistatin plays a critical role in establishing uterine receptivity. Our results contribute to the understanding of the molecular mechanisms underlying uterine receptivity and offer a useful animal model for studying implantation and decidualization failure.

Author contributions: P.T.F., D.M., R.K., and M.M.M. designed research; P.T.F., D.M., and R.K. performed research; P.T.F., D.M., and M.M.M. analyzed data; and P.T.F., D.M., and M.M.M. wrote the paper.

Reviewers: K.L.L., Monash University; and F.P., University of Florence.

The authors declare no conflict of interest.

[1]To whom correspondence should be addressed. Email: mmatzuk@bcm.edu.

This article contains supporting information online at www.pnas.org/lookup/suppl/doi:10.1073/pnas.1620903114/-/DCSupplemental.

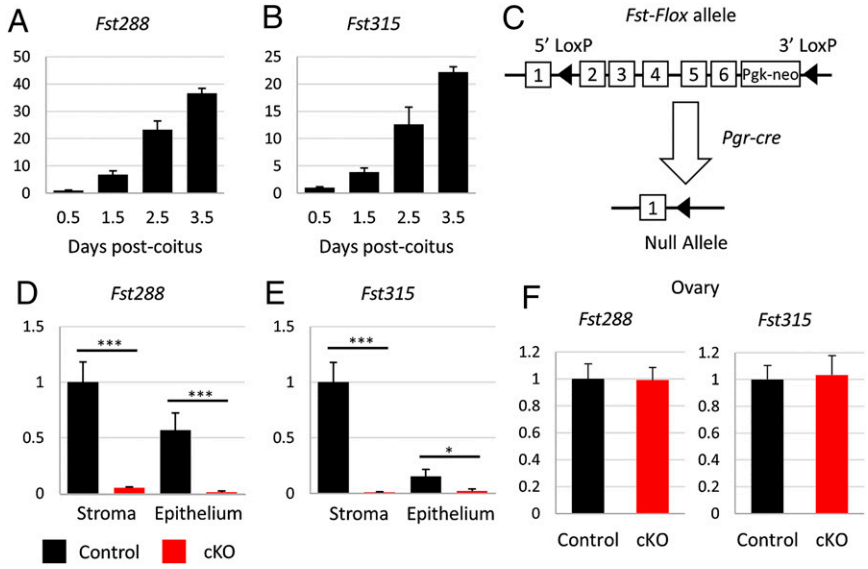

Fig. 1. Generating a conditional knockout of *Fst* in the uterus. (*A* and *B*) Relative *Fst288* and *Fst315* mRNA levels in whole uterus in wild-type females (n = 3 per time point) mated to vasectomized males. Gene-expression data are normalized to levels of 36B4 mRNA with the average value of the 0.5-dpc time point set to one. Data are presented as ± SEM. (*C*) Illustration of the *Fst* conditional allele with *loxP* sites placed in intron 1 and at the 3′ end of exon 6. (*D*–*F*) Relative *Fst288* and *Fst315* mRNA levels in uterine stroma and epithelium at 3.5 dpc (control, n = 3; cKO, n = 6) (*D* and *E*) and in adult ovary (control, n = 4; cKO, n = 4) (*F*). Relative gene-expression data are normalized to levels of 36B4 mRNA with the average value of the control set to one and are compared across genotype. Data are presented as mean ± SEM; $*P < 0.05$, $***P < 0.005$.

Results

Generation of *Fst*-cKO Mice. Previous studies have shown that FST is significantly up-regulated in the mouse uterus during early pregnancy, rising from negligible levels in nonpregnant females to higher levels of expression at the time of blastocyst implantation at 3.5 d post coitum (dpc) (Fig. 1 *A* and *B*) (21, 22). To study the roles of FST in the uterus during pregnancy, we generated mice with conditional deletion of *Fst* in the uterus. To do so, we started with mice carrying homozygous alleles of *Fst* with *loxP* sites placed in intron 1 and at the 3′ end of exon 6 (17). $Fst^{flox/flox}$ mice were mated to mice carrying a *Pgr-cre* allele, in which *Cre* is knocked in to the *Pgr* locus allowing Cre protein expression to be driven by the native *Pgr* promoter (23). We produced $Pgr^{cre/+}$ $Fst^{flox/flox}$ (cKO) mice, in which exons 2 through 6 are excised (Fig. 1*C*), eliminating the expression of FST in tissues expressing the progesterone receptor (PR), i.e., the anterior lobe of pituitary glands, granulosa cells of the postovulatory follicles, oviducts, and epithelium, stroma, and myometrium of the uterus (23). We verified by quantitative RT-PCR (RT-qPCR) that expression of both isoforms of the *Fst* gene are ablated in the uterus of 3.5-dpc pregnant mice (Fig. 1 *D* and *E*). We did not observe any change in *Fst* expression in the ovaries of randomly cycling adult *Fst*-cKO mice (Fig. 1*F*).

***Fst*-cKO Mice Are Severely Subfertile but Display Normal Ovarian Function.** Female fertility was assessed by mating *Fst*-cKO and control females with wild-type males continuously for 4 mo and tracking the number of litters and pups produced by each female. *Fst*-cKO females were severely subfertile, producing significantly fewer pups per female (2% of the control; $P < 0.001$), fewer litters per female ($P < 0.001$), and fewer pups per litter ($P < 0.001$) than the control females (Table 1). Notably, five of nine *Fst*-cKO females were sterile and did not produce any pups during the 4-mo mating trial. The pups that were born to *Fst*-cKO mothers were unremarkable and developed normally from birth to weaning. We observed vaginal plugs in *Fst*-cKO mice indicating that mating behavior was normal in these females. We did not observe gross developmental defects in the uteri of our *Fst*-cKO mice.

Because *Pgr-cre* is expressed in the granulosa cells of preovulatory follicles (23) and FST has been shown to play an important role in the ovary (17), we examined ovarian function in our *Fst*-cKO mice. Histological examination of ovaries from adult females showed no overt differences between *Fst*-cKO and control mice, with corpus luteum observed in both (Fig. S1 *A* and *B*), and superovulation of 3-wk-old mice showed no significant difference in the number of oocytes released (Fig. S1*C*). Oocyte quality is not compromised in *Fst*-cKO females because equivalent numbers of blastocysts were recovered after flushing the uterine horns of 3.5-dpc pregnant control and *Fst*-cKO mice (Fig. S1*D*). Finally, we measured ovarian production of estradiol (E2) and progesterone (P4) during pregnancy by examining serum hormone levels at 3.5 dpc and found no change in *Fst*-cKO mice (Fig. S1 *E* and *F*). Because *Fst*-cKO mice are sterile or severely subfertile but show normal mating behavior, ovarian function, oocyte quality, and hormone levels during pregnancy, we next examined the effects of *Fst* ablation on uterine function during early pregnancy.

***Fst*-cKO Mice Show Impaired Blastocyst Implantation.** Implantation of the embryo into the uterus is an essential step for the establishment of pregnancy. In the mouse, embryo implantation occurs in a stepwise process. Between 3.5 and 4.5 dpc, the blastocyst attaches to the uterine luminal epithelial layer, triggering decidualization—the proliferation and differentiation of stromal cells to prepare for embryo implantation—in the stromal layer (24) and closure of the uterine lumen (25). The number and location of implanted embryos in the uterus can be visualized by intraocular injecting Chicago Blue dye, which intercalates into the vascularized decidual tissue surrounding the implanted embryo and

Table 1. Four-month breeding trial with wild-type males

Genotype	Females	Pups	Pups per female	Litters	Pups per litter
Control	7	184	26.3 ± 1.52	28	6.57 ± 0.71
cKO	9	5	0.56 ± 0.24	4	1.25 ± 0.25

turns the implantation site a vibrant blue color. We assessed implantation in *Fst*-cKO and control mice at 4.5 dpc using this method; control mice had an average of 8.75 ± 0.48 implantation sites per pregnant female, but *Fst*-cKO mice had no implantation sites (Fig. 2 *A*–*C*). Histology of 4.5-dpc uteri from control and *Fst*-cKO mice shows that embryos attach properly to the luminal epithelium and trigger luminal closure in the control mice, but in the *Fst*-cKO mice the embryo does not attach to the luminal epithelium and instead floats in the uncontracted lumen (Fig. 2 *D*–*G*). We were able to observe blastocysts after we flushed the uteri of several *Fst*-cKO mice ($n = 3$) at 4.5 dpc, indicating that the blastocysts had failed to attach to the *Fst*-cKO uterus and that the uterine lumen had not contracted around the embryo. We found a significant decrease in the expression of decidualization genes *Hand2*, *Wnt4*, and *Bmp2*, but not their upstream regulator *Nr2f2* (Fig. 2*H*), supporting our observation that embryos fail to attach to the luminal epithelium of *Fst*-cKO mice and thus do not stimulate a decidual response.

***Fst*-cKO Mice Fail to Achieve Uterine Receptivity.** For the embryo to attach to and implant into the uterus, the uterus must change from a nonreceptive to a receptive state. These changes are regulated by the hormones E2 and P4 and by an intricate series of downstream interactions between the stromal, luminal epithelium, and glandular epithelial layers of the uterus (26). In the uterine luminal epithelium, E2 signals support proliferation of the luminal epithelium, whereas P4 signals oppose proliferation and drive differentiation (27). For the embryo to attach, the luminal epithelium must switch from a nonreceptive proliferative to a receptive differentiated state. Because we observed a failure of attachment and implantation in our *Fst*-cKO mice, we examined proliferation and two key markers of uterine receptivity, mucin 1 (MUC1) and E-cadherin, in the uterine luminal epithelium at 3.5 dpc. MUC1 is down-regulated during epithelial differentiation and must be lost for the mouse uterus to be receptive to embryo attachment (28). Down-regulation of E-cadherin in the luminal epithelial layer is part of the loss of apical–basal polarity, a change necessary to allow embryo attachment (29). In our control mice, the uterus appears receptive without epithelial proliferation, indicated by the lack of Ki67 immunostaining (Fig. 3 *A* and *C*), and with low expression of MUC1 and E-cadherin seen by immunofluorescence (Fig. 3 *E* and *G*). However, histology and immunofluorescence show a nonreceptive phenotype in *Fst*-cKO mice with continued proliferation in the luminal epithelial layer, indicated by positive Ki67 staining (Fig. 3 *A*–*D*) and retention of luminal epithelial expression of MUC1 and E-cadherin (Fig. 3 *E*–*H*).

Because both epithelial proliferation and *Muc1* expression are driven by E2 and are constrained by P4 signaling, we examined gene-expression markers for both E2 and P4 signaling by RT- qPCR. E2 signaling is significantly enhanced in *Fst*-cKO mice at 3.5 dpc with E2 target genes *Lif*, *Ltf*, and *Muc1* up-regulated (Fig. 3*I*). P4 signaling appears to be unaltered with PR-regulated genes *Hand2*, *Nr2f2*, *Ihh*, and *Smo* showing no change in expression (Fig. 3*J*). We did not observe any difference between serum E2 and P4 levels (Fig. S1 *E* and *F*) or between estrogen receptor α (*Esr1*) and PR gene expression levels at 3.5 dpc in control and *Fst*-cKO mice (Fig. 3*K*). This finding suggests that a cofactor may drive an increased response to E2 signaling in the absence of FST and may interfere with the transition of the luminal epithelium from a proliferative to a differentiated state.

To assess the effects of *Fst* knockout on the uterine response to E2 and P4, we performed a Pollard experiment (27), which simulates the hormonal changes that accompany pregnancy leading up to uterine receptivity and allows the study of a specific time point after the E2+P4 surge that initiates the receptive phase (Fig. 4*A*). At 16 h after E2+P4 treatment, we observed changes in gene expression similar to those seen at 3.5 dpc with up-regulation of E2 target genes (Fig. S2*A*) and no change in P4-regulated genes (Fig. S2*B*). We also observed aberrant proliferation in the luminal epithelium of *Fst*-cKO mice in line with the data from 3.5-dpc pregnant females as measured by Ki67 immunoreactivity (Fig. S2 *C* and *D*). A possible mechanism for the aberrant luminal epithelial

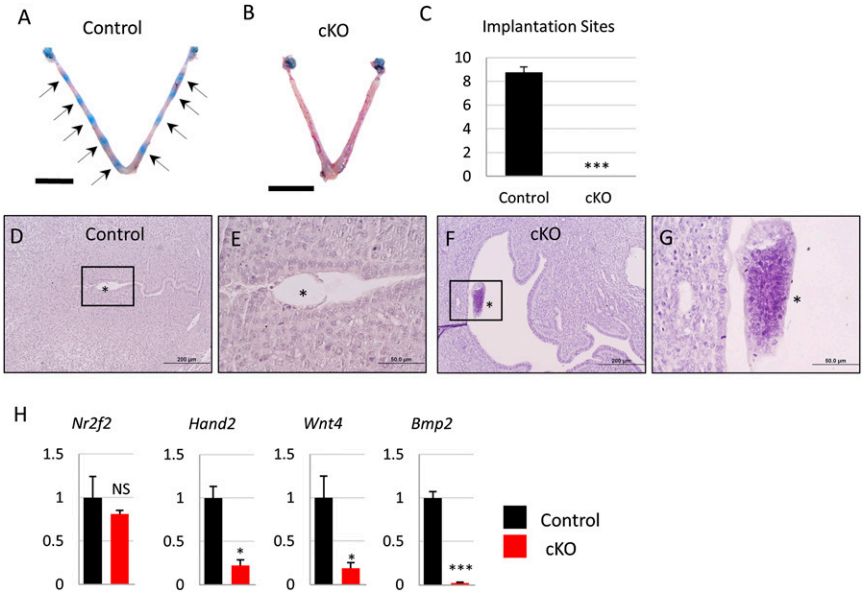

Fig. 2. Embryo implantation at 4.5 dpc is absent in *Fst*-cKO mice. (*A* and *B*) Implantation sites were visualized at 4.5 dpc by intraocular injection of females with Chicago Blue dye. Black arrows indicate implantation sites. (*C*) The number of implantation sites visible as blue bands by Chicago Blue dye in control ($n = 4$) and *Fst*-cKO females ($n = 11$) was counted and is reported as mean ± SEM. (*D* and *E*) H&E staining of implantation sites and uterus from control and *Fst*-cKO mice. (*F* and *G*) Higher magnification of boxed areas of *D* and *E*. Asterisks indicate embryos. (*H*) Gene-expression data comparing relative mRNA levels in implantation sites or uterus at 4.5 dpc (control, $n = 3$; cKO, $n = 3$). Gene-expression data are normalized to levels of 36B4 mRNA with the average value of the control set to one and are compared across genotype. Data are presented as mean ± SEM; $^*P < 0.05$, $^{***}P < 0.005$. (Scale bars: *A* and *B*, 1 cm; *D* and *F*, 200 μm; *E* and *G*, 50 μm.) NS, not significant.

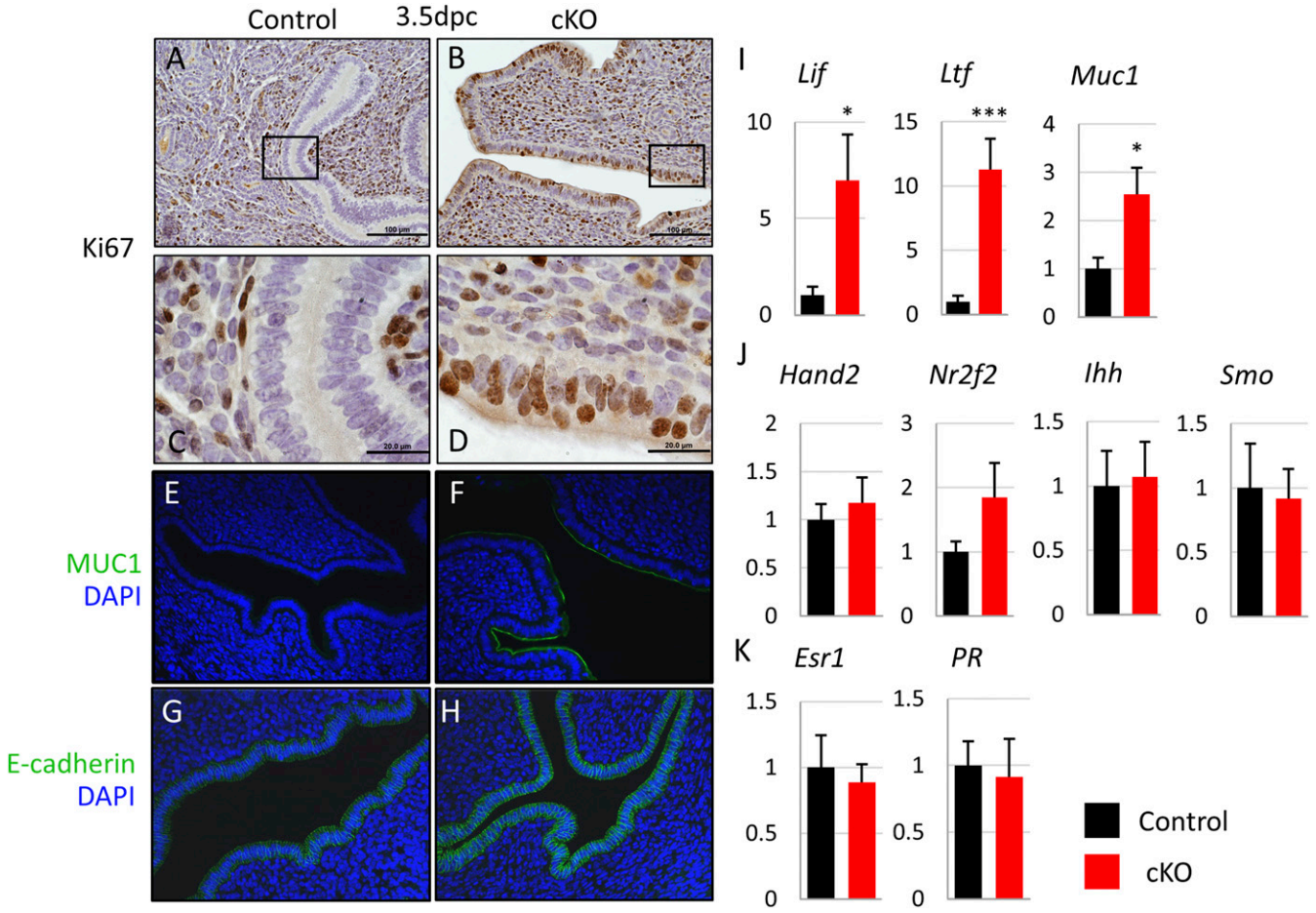

Fig. 3. *Fst*-cKO mice fail to achieve uterine receptivity at 3.5 dpc. (*A*–*D*) Immunohistochemistry for the proliferation marker Ki67 with paraffin sections from pregnant control and *Fst*-cKO females at 3.5 dpc. Sections are counterstained with hematoxylin. Brown staining denotes Ki67$^+$ proliferating cells. (*C* and *D*) Higher magnification of the boxed sections in *A* and *B*. (Scale bars: *A* and *B*, 100 μm; *C* and *D*, 20 μm.) (*E* and *F*) Immunofluorescence for the uterine receptivity marker MUC1 (green) and nuclear marker DAPI (blue). Expression of MUC1 in the epithelium at 3.5 dpc indicates a nonreceptive uterus. (*G* and *H*) Immunofluorescence for the uterine receptivity marker E-cadherin (green) and nuclear marker DAPI (blue). Expression of E-cadherin in the epithelium at 3.5 dpc indicates intact apical–basal polarity and a nonreceptive uterus. (Magnification: 20×.) (*I*–*K*) Relative expression of mRNA for E2- (*I*) and P4- (*J*) regulated genes and hormone receptors (*K*) in control ($n = 3$) and *Fst*-cKO ($n = 6$) females at 3.5 dpc. Uterine luminal epithelium and stroma were separated and purified after trypsin digestion. *Lif*, *Ltf*, *Muc1*, and *Ihh* are epithelial-expressed genes; *Hand2*, *Nr2f2*, *Smo*, *Esr1*, and *PR* are stromal-expressed genes. Gene-expression data are normalized to levels of 36B4 mRNA with the average value of the control set to one and are compared across genotype. Data are presented as mean ± SEM; $*P < 0.05$, $***P < 0.005$.

proliferation seen in *Fst*-cKO mice was detectable in the Pollard experiment. The proproliferation genes *Mcm2*, *Mcm7*, and *Klf4* were up-regulated, whereas the negative regulator *Klf15* was down-regulated (Fig. 4*B*). BMP signaling through ALK3 supports P4 signaling in the luminal epithelium through binding of SMAD4 and PR at *Klf15* to up-regulate its expression, leading to down-regulation of *Mcm2* and *Mcm7* by KLF15 and reducing proliferation in the luminal epithelium (4).

***Fst*-cKO Mice Have Impaired Decidualization.** Although we were unable to observe any implantation sites in *Fst*-cKO mice, the up-regulation of FST at 5.5 dpc in normal pregnancy (22) suggests that it might play an important role in decidualization. To address this hypothesis, we studied the role of FST in decidualization using an artificial decidualization experiment (Fig. 5*A*). In artificial decidualization, the hormonal profile of pregnancy is simulated in ovariectomized mice, and decidualization is triggered by injection of sesame seed oil into the uterine lumen of one of the two uterine horns. Injecting oil disrupts the epithelial layer in a manner similar to embryo attachment and triggers decidualization. The decidual response is promoted by additional hormone treatments, and after 5 d the untreated and oil-injected uterine horns of each mouse are examined. Although ablation of *Fst* did not entirely preclude decidualization in our assay, it did severely compromise it. *Fst*-cKO mice had a significantly diminished response to the decidual stimuli (Fig. 5 *B*–*D*) characterized by dramatically reduced proliferation (Fig. 5 *E* and *F*). Stromal differentiation was also poor in *Fst*-cKO mice, with smaller, less-differentiated stromal cells detected by alkaline-phosphatase staining (Fig. 5 *G* and *H*).

Loss of Uterine FST Leads to Aberrant Activin Signaling During Early Pregnancy. Given that FST regulates activin and BMP signaling, we assessed the impact of uterine *Fst* knockout on activin and BMP expression and activity. We observed a striking up-regulation of inhibin βB transcript levels in *Fst*-cKO mice at 3.5 dpc, 4.5 dpc, and 16 h after treatment with E2+P4 (Fig. 6*A*), but not of inhibin βA or inhibin α transcripts (Fig. S2*E*). In line with the changes that we observed in gene expression, inhibin βB protein expression is up-regulated in the uteri of pregnant *Fst*-cKO females at 3.5 dpc (Fig. 6 *B* and *C*). Homodimers of inhibin βB form activin B, which binds to a complex of ACVR2A/B and ALK4/7 and drives changes in gene expression through phosphorylation of SMAD2/3.

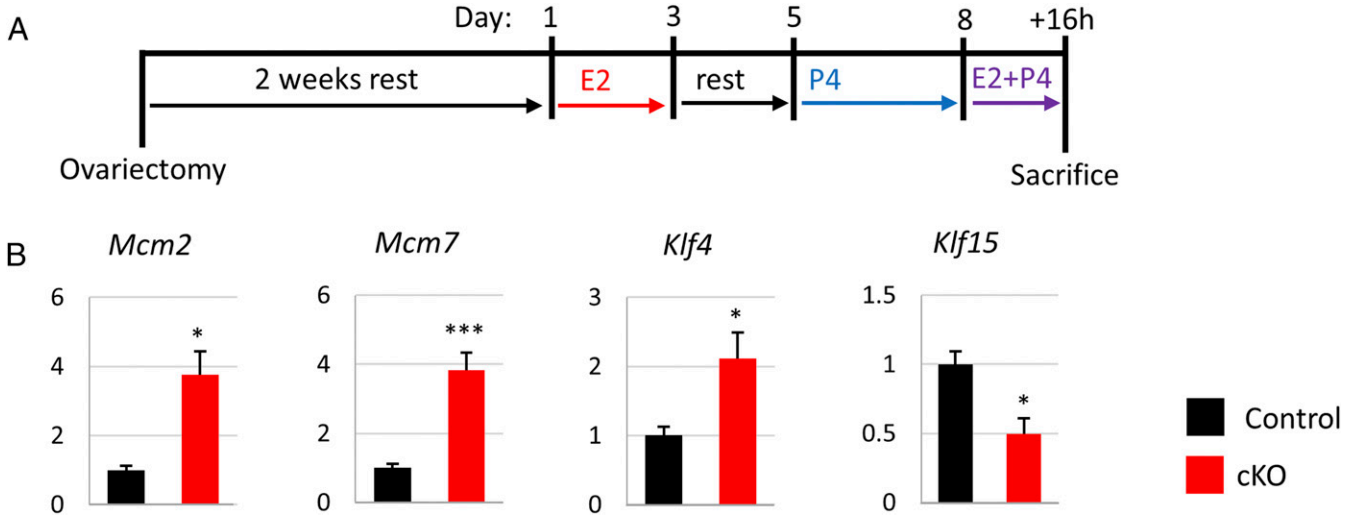

Fig. 4. *Fst*-cKO mice do not respond properly to E2+P4 treatment. (*A*) Experimental plan outline. (*B*) Uterine luminal epithelium and stroma were separated and purified after trypsin digestion. Analysis of the epithelial fraction (control, $n = 3$; cKO, $n = 5$) is presented in *B*. Gene-expression data are normalized to levels of 36B4 mRNA with the average value of the control set to one and are compared across genotype. Data are presented as mean ± SEM; $*P < 0.05$, $***P < 0.005$.

We observed an increase in phosphorylated SMAD2/3 protein by Western blot in the uteri of *Fst*-cKO mice at 3.5 dpc (Fig. 6 *D* and *F*).

The other major targets of FST expressed in the uterus at this time point are the BMPs. To determine whether BMP levels were altered in the absence of FST, we examined gene expression of *Bmp2*, *Bmp5*, and *Bmp7* at 3.5 dpc but found no change (Fig. S2*F*). To check for any global effect on BMP signaling, we immunoblotted for phosphorylated SMAD1/5, the effector of BMP signaling, and found a decrease in the uteri of *Fst*-cKO mice at 3.5 dpc (Fig. 6 *E* and *G*). To assess the effect of reduced phosphorylated SMAD1/5 on SMAD binding to BMP signaling targets, we performed ChIP for SMAD4 and PR at their shared binding site in *Klf15* (4). We observed no change in PR occupancy; however, we observed a significant reduction in SMAD4 binding to *Klf15* in *Fst*-cKO mice (Fig. 7).

Together, our data on activin and BMP signaling support the hypothesis that FST suppresses activin B activity and *Inhbb* expression during early pregnancy, allowing BMP signaling to predominate (Fig. 8*A*). In the absence of FST, activin B is up-regulated, and

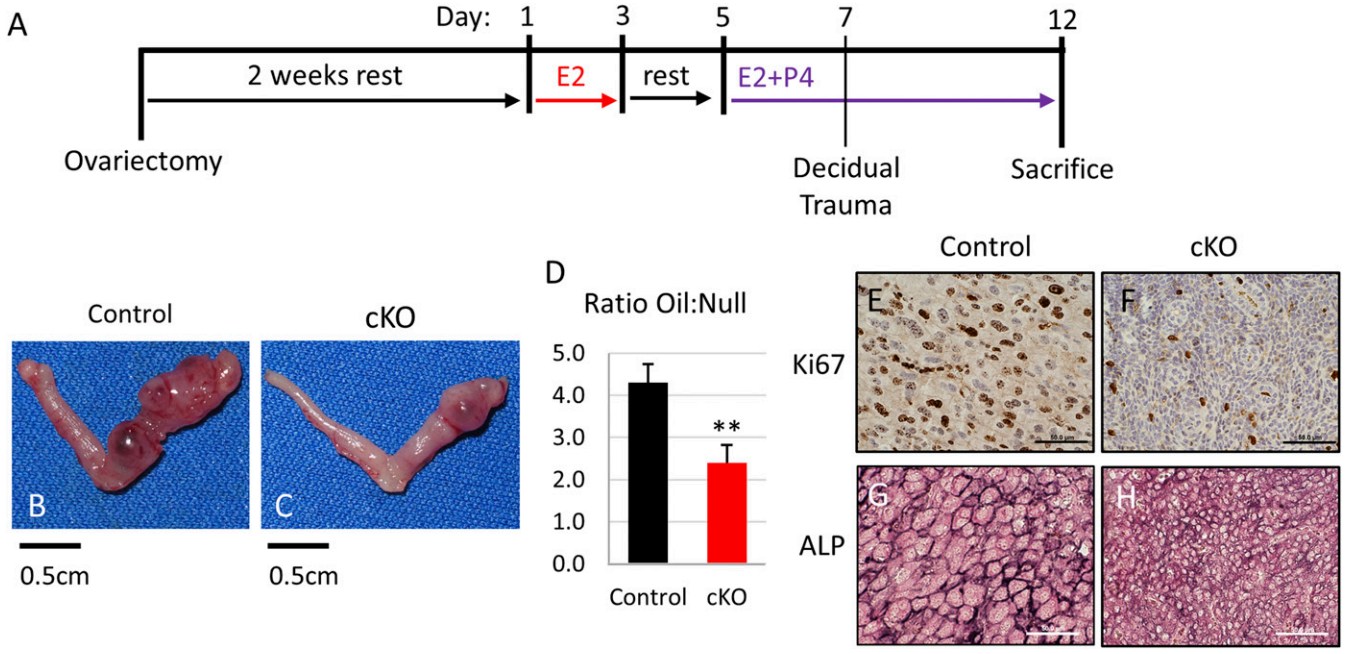

Fig. 5. *Fst*-cKO mice have defective decidualization. (*A*) Experimental plan outline. (*B* and *C*) Representative pictures showing the gross morphology of oil-treated uterine horns (*C*) and untreated horns (*B*) from control and *Fst*-cKO mice collected 5 d after oil injection. (*D*) The ratio between the wet weight of the oil-treated horn to the wet weight of the untreated horn was calculated for each control ($n = 6$) and each *Fst*-cKO ($n = 3$) mouse; then ratios were averaged and compared across genotype. Data are presented as mean ± SEM; $**P < 0.01$. (*E* and *F*) Immunohistochemistry for the proliferation marker Ki67 with paraffin sections from the oil-treated horns of control and *Fst*-cKO females. Sections were counterstained with hematoxylin. Brown staining denotes $Ki67^+$ proliferating cells. (*G* and *H*) Immunohistochemistry for the stromal differentiation marker alkaline phosphatase with cryo-sections from the oil-treated horns of control and *Fst*-cKO females. Dark staining indicates alkaline phosphatase expression. (Scale bars: *E*–*H*, 50 μm.) ALP, alkaline phosphatase.

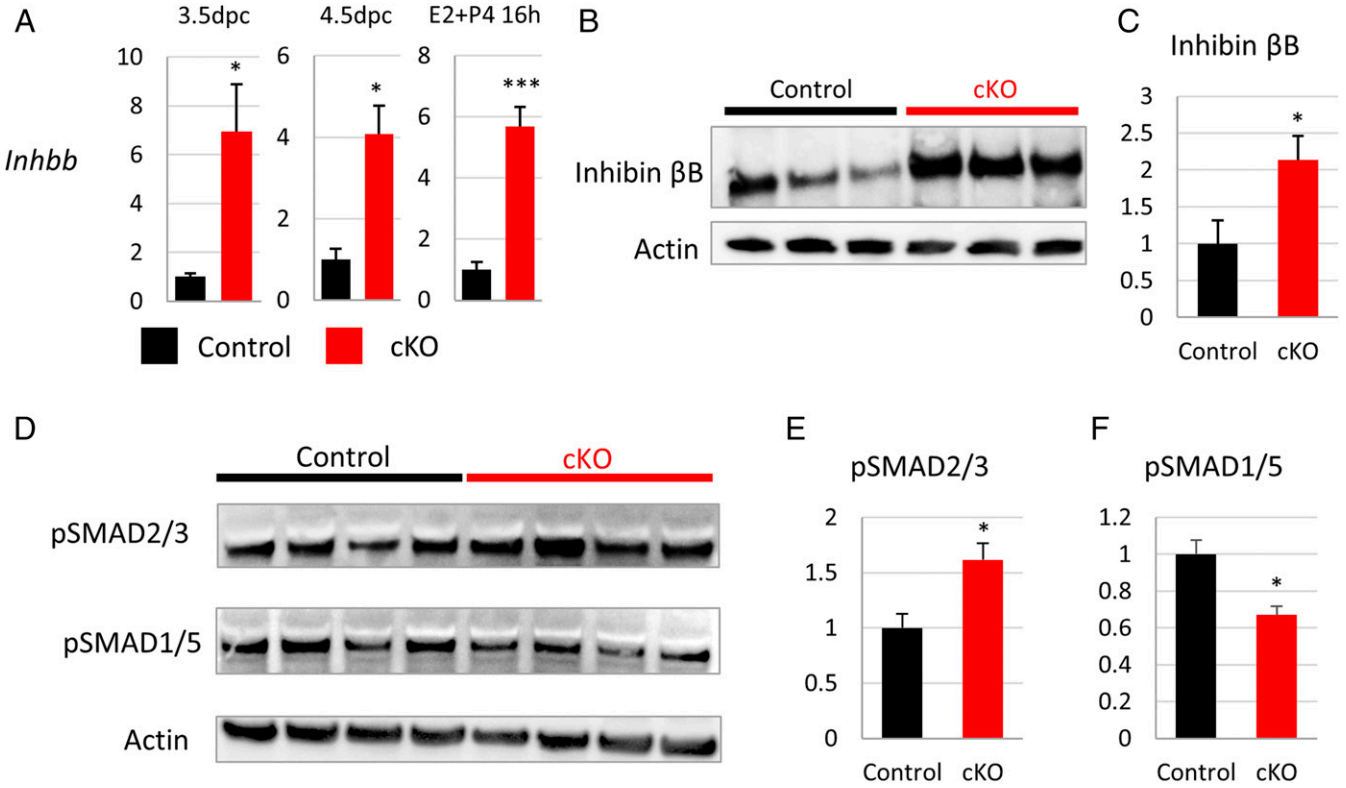

Fig. 6. Activin expression and signaling are up-regulated in early pregnancy of *Fst*-cKO mice. (*A*) Expression of *Inhbb* mRNA levels at 3.5 dpc in the stromal fraction (control $n = 3$, cKO $n = 6$), at 4.5 dpc in whole uterus (control $n = 3$, cKO $n = 3$), and 16 h after E2+P4 treatment in the stromal fraction (control $n = 4$, cKO $n = 4$). Gene-expression data are normalized to levels of 36B4 mRNA with the average value of the control set to one and are compared across genotype. (*B*) Western blot analysis for inhibin βB of whole uteri from pregnant control ($n = 3$) and *Fst*-cKO females ($n = 3$) at 3.5 dpc. (*C*) Quantification of the Western blot shown in *B*, normalized to actin. (*D*) Western blot analysis for pSMAD2/3 and pSMAD1/5 of whole uteri from pregnant control ($n = 4$) and *Fst*-cKO females ($n = 4$) at 3.5 dpc. (*E* and *F*) Quantification of the Western blots shown in *D* normalized to actin. Data are presented as mean ± SEM; $*P < 0.05$, $***P < 0.005$.

competition for shared signaling pathway components between activin and BMP signaling likely reduces the BMP signals critical for uterine receptivity (Fig. 8*B*).

Discussion

In this study, we generated a mouse model with conditional ablation of *Fst* in the uterus. Uterine *Fst*-cKO mice are sterile or severely subfertile because they fail to achieve uterine receptivity to allow embryo implantation and cannot properly decidualize to support an implanted embryo. FST has been shown to be critical for ovarian function by conditional ablation in the ovary (17) and to be implicated in uterine development through studies of mice with systemic expression of only one of the two isoforms of FST (18–20); our study examines the role of FST in the uterus during pregnancy. In agreement with previous studies (21, 22), we found that *Fst* is strongly up-regulated during early pregnancy. In the absence of *Fst*, we discovered that the uterine luminal epithelium does not respond properly to E2 and P4 signals, remaining unreceptive to embryo attachment by continuing to proliferate and failing to differentiate.

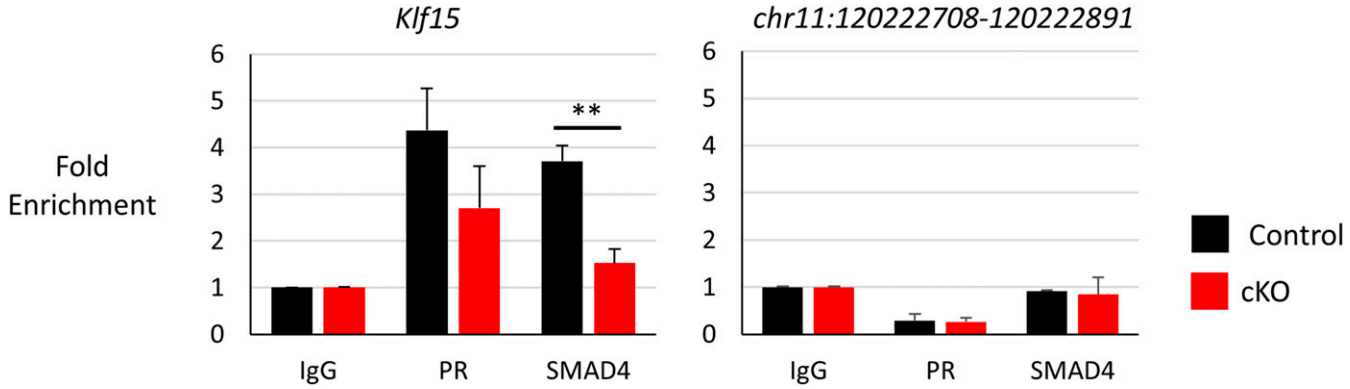

Fig. 7. SMAD4 binding to *Klf15* is down-regulated in *Fst*-cKO mice at 3.5 dpc. ChIP-qPCR was used to analyze the binding of PR and SMAD4 to their binding sites at *Klf15* (*Left*) and at chr11:120222708–120222891 (*Right*), a negative control region. Data were normalized to input and are expressed as mean fold enrichment over input relative to an IgG control, ± SEM; $**P < 0.01$.

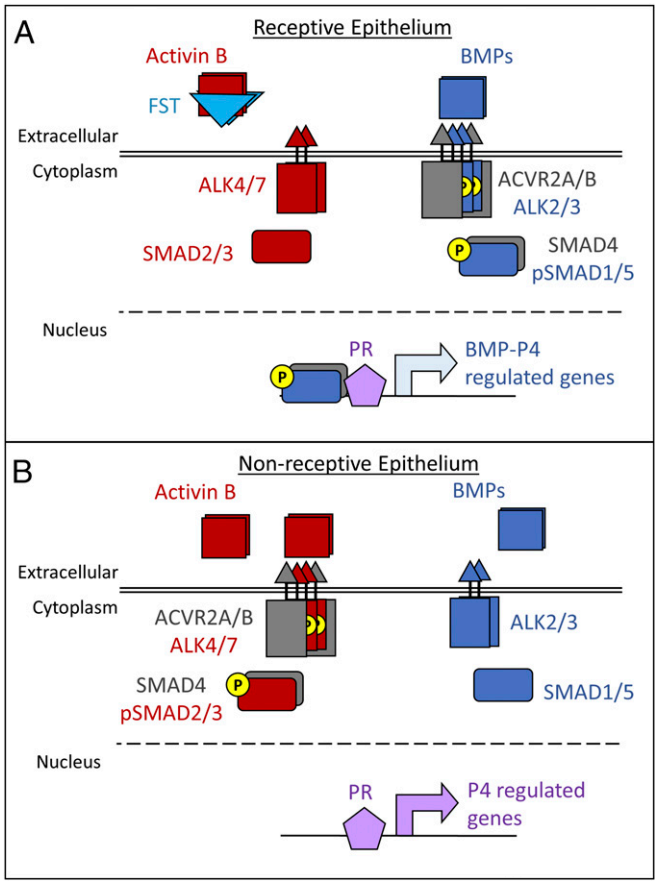

Fig. 8. FST promotes uterine receptivity by regulating activin and BMP signals. (*A*) Normally, FST suppresses the action and expression of activin B during early pregnancy. This suppression allows BMP signaling to be the primary partner for the shared type 2 receptors, ACVR2A/B, and the shared cofactor, SMAD4. BMP signaling cooperates with P4 signaling through interactions with PR to promote a receptive uterine epithelium. (*B*) When FST is conditionally ablated in the uterus, the process depicted in *A* is disrupted. Uninhibited and up-regulated activin B competes with BMP signaling for the shared ACVR2A/B and SMAD4, driving activin signaling at the expense of the BMP signaling necessary for uterine receptivity.

We hypothesize that the failure of uterine receptivity is caused by increased expression and activity of inhibin βB in the absence of FST during early pregnancy. Inhibin βB dimerizes to form activin B, a TGFβ family ligand that signals through ACVR2A/B and ALK4/7 to drive phosphorylation of SMAD2/3, which regulate transcription. The aberrant activin expression that we observed in the absence of FST is likely responsible for reduced BMP signaling at 3.5 dpc. Antagonism between signaling by the TGFβ/activin and BMP families of ligands has been reported in numerous developmental processes (30–32) and tissues (33–38). Dysregulation of this antagonism can have dramatic consequences for tissue homeostasis, as seen in juvenile granulosa cell tumors, in which mouse models have shown that tumorigenesis is promoted by TGFβ/activin signaling through SMAD2/3 and is opposed by BMP signaling through SMAD1/5 (39–47). Direct competition between the pathways can occur for availability of the shared type 2 receptors ACVR2A/B (48–50) or the availability of the common cofactor SMAD4 (51). In the context of uterine receptivity, our findings suggest that FST likely promotes BMP signaling critical for receptivity (4) by preventing or reducing activin competition (Fig. 8); although FST has been shown to bind BMPs, it has a much higher affinity for activins (52).

Another TGFβ ligand expressed during the peri-implantation period in the uterus is nodal, which signals through ACVR2A/B with the assistance of its coreceptor cripto. *Nodal* is expressed in the uterine glandular epithelium at 3.5 dpc and may play a role in regulating implantation site spacing (53). *Pgr-cre Nodal*-cKO mice have midgestation pregnancy defects and a reduced rate of pregnancy; however, the early pregnancy defect has not been characterized (54). Although nodal is not regulated by FST, the cripto coreceptor can reduce the strength of activin signals through ACVR2A/B (55). However, because cripto cannot compensate for the absence of FST, the two regulators appear to have nonoverlapping or nonredundant roles during early pregnancy. Future studies are needed to characterize the roles of specific ACVR2A/B ligands, including nodal, more thoroughly during early pregnancy.

We observed increased expression of E2-regulated genes in *Fst*-cKO mice during early pregnancy. This increase may be caused by aberrant activin signaling, because SMAD3 can interact directly with estrogen receptor α to amplify E2 signals (56). Additionally, in mouse uterine tissues treated with estrogen, estrogen receptor α binds to the *Inhbb* promoter regions 2,720 bp upstream of the transcription start site (57). These data suggest that the elevated E2 signaling observed in the absence of uterine FST may contribute directly to maintaining elevated uterine activin B through a positive feedback loop. Therefore, it seems plausible that the absence of uterine FST precludes uterine receptivity because aberrant activin signaling from the stroma to the luminal epithelium dysregulates the uterine response to E2 and P4 by boosting the E2 signal through interactions of phosphorylated SMAD3 with estrogen receptor α. Therefore, we propose that FST repression of activin signaling during early pregnancy has a twofold role: preserving BMP signaling and preventing dysregulation of E2 signaling. Additional studies will be necessary to determine whether aberrant activin expression and activity during early pregnancy in the absence of FST alters E2 signaling directly through SMAD-ERα protein–protein interactions or indirectly by regulating overlapping sets of genes.

We also found that uterine *Fst*-cKO mice have defective decidualization with reduced stromal proliferation and differentiation. Our study provides experimental in vivo evidence that FST plays a critical role in regulating decidualization.

Activin signaling has been implicated as a regulator of decidualization in women; components of activin signaling are expressed in the human endometrium (58), and activins and FST are up-regulated in decidualized stromal cells (59), Activin A is up-regulated during the secretory phase of the menstrual cycle (60), and treatment of artificially decidualized cultured human endometrial stromal cells with exogenous activin A promotes prolactin expression (61), whereas treatment with FST reduces IGFBP-1 secretion (62). Studies of activin expression patterns during decidualization in mice and rats have further suggested that activin expression may regulate decidual regression during placentation (22, 63, 64), and activin signaling is thought to regulate interactions between the fetal placenta and maternal decidua in humans (65, 66); however, the roles of activin signaling in the decidua have not been well studied experimentally in vivo.

Our data showing that FST expression is necessary for a proper decidual reaction suggest that activin is not simply a prodecidualization factor. This notion is further supported by the absence of any gross defects in decidualization in mice deficient for either of the activin type 1 receptors, *Alk7* (67) or *Alk4* (68). Although the absence of such defects could result from redundancy between the two receptors, uterine conditional knockout of either *Alk2* (3) or *Alk3* (4), the type 1 receptors for the critical decidualization factor BMP2 (2), severely compromises decidualization. We cannot comment on the roles of maternal FST in regulating placentation because uterine receptivity defects preclude any study of placentation in our *Fst*-cKO mice. New in vivo models, particularly with uterine conditional knockout or overexpression of inhibin βA/B,

are needed to study the roles of activin signaling in the decidua and to determine whether FST and activins can serve as biomarkers for uterine receptivity.

Aberrant levels of uterine FST, activins, and inhibins are reported in women with recurrent miscarriage (11, 12), repeated implantation failure after in vitro fertilization (14), and impending abortion during early pregnancy (10). Our study suggests that regulation of activin signaling by FST during early pregnancy may play important roles in uterine receptivity and decidualization, critical events for the success of early pregnancy. In the United States, ∼12% of women have difficulty becoming pregnant or carrying a pregnancy to term (69). Assisted reproductive technology (ART) can help many women with infertility; however, ART success rates are low, with an ∼30% chance of a live birth per procedure (70). Embryo implantation into the uterus is a significant bottleneck to improving ART success rates; ∼48% of in vitro fertilization attempts fail to achieve implantation, and a third of implanted embryos are lost before clinical pregnancy (71). Additional studies are necessary to determine whether FST and activin levels could serve as biomarkers for in vitro fertilization success or as the basis for treatments to improve implantation rates of in vitro fertilization.

Materials and Methods

Animals and Ethics Statement. All mouse lines were maintained on a hybrid C57BL/6J and 129S5/SvEvBrd genetic background. Animal handling and surgeries were performed per the NIH *Guide for the Care and Use of Laboratory Animals* (72) and were approved by the Institutional Animal Care and Use Committee of Baylor College of Medicine.

Generation of *Fst*-cKO Female Mice. Mice with floxed alleles of *Fst* (originally $Fst^{tm2Zuk/tm2Zuk}$, here $Fst^{flox/flox}$) have been previously described (17). $Fst^{flox/flox}$ mice were bred with $Pgr^{cre/+}$ mice (23) to generate $Pgr^{cre/+}$ $Fst^{flox/+}$ males. These males then were bred with $Fst^{flox/flox}$ females to produce $Pgr^{cre/+}$ $Fst^{flox/flox}$ males. Our experimental $Pgr^{cre/+}$ $Fst^{flox/flox}$ and littermate control $Fst^{flox/flox}$ females were then produced by breeding $Pgr^{cre/+}$ $Fst^{flox/flox}$ males with $Fst^{flox/flox}$ females. Mice were genotyped by PCR analysis of genomic DNA isolated from tail clippings.

Fertility Analysis. Female fertility was assessed by mating cohorts of *Fst* cKO experimental ($n = 9$) and control ($n = 7$) females individually starting at 6 wk of age with sexually mature males. The numbers of litters and pups were tracked over a 4-mo period for each mouse. Pups per female and pups per litter for each genotype are reported as mean ± SEM.

Timed Mating. Sexually mature mice (6 wk of age or older) were mated to fertile wild-type males and copulation was confirmed by the observation of vaginal plugs the following morning. The morning when the plug was observed is designated as 0.5 dpc.

Visualizing Implantation Sites. Implantation sites were visualized in 4.5 dpc pregnant mice by retro-orbital injection of 200 μL of 1% Chicago Blue B; mice were killed ∼2 mo after injection. Dissected uteri were photographed, and the blue bands indicating implantation sites were counted.

Blastocyst Collection. Blastocysts were isolated from 3.5-dpc pregnant mice by dissecting out the uterus, isolating each horn, inserting a 26-gauge needle into the lumen of the uterine horn through the oviduct, flushing 200 μL of HBSS (Invitrogen) into each horn, collecting the flushed medium from both horns on a tissue culture plate, and counting the number of blastocysts under a dissecting microscope.

Ovulation Analysis. Female mice at age 20–23 d were injected with 5 IU pregnant mare serum gonadotropin (PMSG), followed by 5 IU human chorionic gonadotropin (hCG) 44–46 h later. After an additional 18–22 h, the mice were killed, and oviducts were isolated. Cumulus-oocyte complexes (COC) were removed from the oviducts and collected in M2 medium (Sigma-Aldrich). The number of COCs per female was counted and compared across genotypes.

Hormone Analysis. Blood was collected by cardiac puncture from 3.5-dpc pregnant females under isoflurane anesthesia immediately before mice were killed. Pregnancy was verified by flushing the uteri of mice at 3.5 dpc and observing blastocysts. Serum was separated from the blood by centrifugation and stored at −80 °C before hormone analysis. Serum P4 and E2 levels were measured by the Ligand Assay and Analysis Core at University of Virginia.

Pollard Experiment. The hormonal profile of pregnancy at the time of implantation was simulated using a previously described experimental scheme (27) which we refer to as the "Pollard" experiment. In brief, mice at 6–8 wk of age were ovariectomized under isoflurane anesthesia with appropriate analgesics. After at least 2 wk to allow endogenous ovarian hormones to dissipate completely, the mice were treated with daily s.c. injections of E2 (100 ng) for 2 d. Following this treatment and after 2 d of rest, the mice were injected daily for 3 d with 1 mg of P4. On the fourth day, the mice were treated with 100 ng of E2 and 1 mg of P4. The mice were killed 16 h after the E2+P4 injection.

Artificial Induction of Decidualization. Decidualization was artificially induced using previously described methods (73). In brief, mice at 6–8 wk of age were ovariectomized under isoflurane anesthesia with appropriate analgesics. After at least 2 wk to allow endogenous ovarian hormones to dissipate completely, the mice were treated daily with s.c. injections of E2 (100 ng) for 2 d. After 2 d of rest, the mice were treated daily with 1 mg P4 s.c. and 10 ng of E2 s.c. for 3 d. A second surgery was performed 6 h after the last hormone injection to expose one uterine horn. Decidualization was induced in this horn by injection of 100 μL of sesame oil into the lumen. The other uterine horn was left untreated as a control. Daily hormone treatments with 1 mg P4 s.c. and 10 ng E2 s.c. were continued for 5 d. The mice were killed 6 h after the last hormone injection, and the wet weights of the traumatized and control uterine horns of each mouse were recorded. Uterine tissue was collected from both horns and was fixed in 10% neutral buffered formalin or was frozen. Fixed samples were processed and embedded in paraffin blocks or were run through a sucrose gradient before freezing.

Epithelial–Stromal Separation. To separate the luminal epithelium from the stromal compartment of the uterus at 3.5 dpc of pregnancy or in the Pollard experiment, uteri were collected, cut into 2-mm pieces, and incubated in 1% trypsin (Sigma-Aldrich) in HBSS (Invitrogen) for 30 min at 37 °C. After incubation, the luminal epithelium was visualized under a dissecting microscope and isolated using forceps and a mouth pipette. Both epithelial and stromal samples were frozen for RNA extraction. The purity of the epithelial and stromal samples was verified by evaluating epithelial (keratin 8, *Krt8*) and stromal (vimentin, *Vim*) markers using RT-qPCR (Fig. S2*G*).

Histological Analysis. Tissues were fixed in 10% neutral buffered formalin for 24 h, transferred to 70% ethanol, and embedded in paraffin. Paraffin sections were stained with H&E or hematoxylin-periodic acid Schiff (PAS) using standard procedures.

Immunofluorescence and Immunohistochemistry. Paraffin sections were deparaffinized with Histo-Clear (Thermo Fisher), hydrated with an ethanol gradient, and boiled for antigen retrieval. After blocking with 5% IgG-free BSA (Sigma-Aldrich) for 1 h at room temperature, sections were incubated overnight at 4 °C with the primary antibodies listed in Table S1. For immunofluorescence, after washing with Tris-buffered saline (TBS) and Tween 20 (TBST), sections were incubated with Alexa Fluor 488-conjugated secondary antibodies (Life Technologies) for 1 h at room temperature, incubated for 5 min with 1:1,000 DAPI in TBST, and mounted with Immu-Mount. For immunohistochemistry, sections were incubated with biotinylated secondary antibodies and ABC reagent (Vector Laboratories), developed using a 3,3′-diaminobenzidine (DAB) substrate kit (Vector Laboratories), and counterstained with H&E.

Alkaline Phosphatase Activity Assay. Uteri from the artificial decidualization experiment were fixed overnight in 10% neutral buffered formalin followed by incubation in a sucrose gradient and were embedded in optimum cutting temperature (OCT) medium using an ethanol/dry ice bath. Frozen sections (5 μm thickness) were postfixed in 0.2% glutaraldehyde for 10 min, washed in 0.1 M Tris·HCl (pH 9.5), and then incubated in 4-nitro blue tetrazolium/5-bromo-4-chloro-3-indolyl-phosphate (NBT/BCIP) working solution (Vector Laboratories) for 15–25 min. Sections were counterstained in Nuclear Fast Red (Vector Laboratories) for 30 s, rinsed in tap water, dehydrated, and then mounted with Permount. A dark blue stain is indicative of alkaline phosphatase activity in the decidualized cells of the uterine stroma.

Western Blot Analysis. Protein was isolated by lysing cells with radio immunoprecipitation assay (RIPA) lysis buffer (Pierce) supplemented by cOmplete EDTA-free protease inhibitor (Roche) or Halt Protease and Phosphatase Inhibitor Mixture (Thermo Fisher). The supernatant was extracted after high-speed centrifugation at 4 °C. Protein was prepared for SDS/PAGE by dilution with 4× Nu-PAGE Sample buffer (Invitrogen), the addition of 2-mercapaethanol (Sigma), boiling, and cooling. SDS/PAGE was performed on NuPAGE 4–12% Bis-Tris gels (Life Technologies) with NuPAGE Mes SDS Running buffer (Life Technologies). Proteins were transferred to PVDF membranes, blocked with 3% milk in Tris-buffered saline and 0.1% Tween 20, probed with protein-specific antibodies, incubated with HRP-conjugated secondary antibodies, and visualized via enhanced chemiluminescence using Super-Signal West Pico Chemiluminescent Substrate (Thermo Scientific) or Super-Signal West Femto Chemiluminescent Substrate (Thermo Scientific). Primary antibodies used in this study are listed in Table S1. All antibodies were diluted in 5% IgG-free BSA in Tris-buffered saline and 0.1% Tween 20. Quantification was performed using the ImageJ gel analysis tool and normalized to actin.

RNA Isolation and RT-qPCR. Gene expression was analyzed by reverse RT-qPCR using a LightCycler 480 II (Roche) and SYBR Green PCR Master Mix (Invitrogen). Results presented were repeated in three or more independent experiments. Melt curve analysis was performed when using SYBR Green to verify a single amplification peak. Primer sequences are listed in Table S2. Changes in gene expression were normalized to the endogenous control 36B4 and calculated using the $2^{\Delta\Delta Ct}$ method with error reported as ± SEM. Comparisons between genotypes are normalized with the control samples set to an average RQ value of one.

SMAD4 and PR ChIP Followed by qPCR. For SMAD4 and PR ChIP followed by qPCR (ChIP-qPCR), uteri at 3.5 dpc from control ($n = 3$) and *Fst*-cKO ($n = 4$) mice were submerged in 1% paraformaldehyde dissolved in 1× PBS and were cut into 3- to 4-mm sections. Tissues were transferred to a 15-mL conical tube and fixed for 15 min on a rocker, quenched in 0.125 M glycine, and washed three times with cold 1× PBS. Liquid was removed, and tissues were flash frozen. ChIP was performed following a modified protocol described in ref. 74. Fixed tissues were lysed in buffer 1 [50 mM Hepes-KOH (pH 7.5), 140 mM NaCl, 1 mM EDTA, 10% glycerol, 0.5% Nonidet P-40, 0.25% Triton X-100] plus cOmplete Protease Inhibitor Mixture (Roche) and were pulverized with a tissue homogenizer. Lysate was incubated for 10 min at 4 °C on a rocker. After centrifugation at 1,650 × *g* for 5 min, tissues were resuspended in lysis buffer 2 [10 mM Tris·HCl (pH 8.0), 200 mM NaCl, 1 mM EDTA, 0.5 mM EGTA] plus cOmplete Protease Inhibitor Mixture (Roche) and were incubated for 10 min at 4 °C on a rocker. After centrifugation, as before, the pellet was resuspended in lysis buffer 3 [10 mM Tris·HCl (pH 8), 100 mM NaCl, 1 mM EDTA, 0.5 mM EGTA, 0.1% Na-Deoxycholate, 0.5% *N*-lauroylsarcosine] and was sonicated. Chromatin was cleared by centrifugation at 13,0000 × *g* at 4 °C, and 10% Triton-X (Sigma) was added. An aliquot of lysate was taken as input and stored at −20 °C. Chromatin was equally divided into four tubes and incubated overnight with antibodies on an orbital shaker at 4 °C. We used 5 μg of rabbit polyclonal PR antibody (sc7208; Santa Cruz) (75), 5 μg of goat polyclonal SMAD4 antibody (AF2097; R&D) (76), and IgG (Sigma). Dynabeads (Life Technologies) were used to capture the protein/DNA/antibody complexes for 4 h on an orbital shaker at 4 °C. Dynabeads then were washed five times with RIPA buffer [50 mM Hepes-KOH (pH 7.5), 500 mM LiCl, 1 mM EDTA, 1% Nonidet P-40, 0.7% Na-Deoxycholate] followed by a final wash in Tris-EDTA (TE) buffer [10 mM Tris·HCl (pH 8), 1 mM EDTA] plus 50 mM NaCl. Protein/DNA complexes were eluted from the magnetic beads [50 mM Tris·HCl (pH 8), 10 mM EDTA, 1% SDS] at 65 °C followed by crosslink reversal overnight at 65 °C. Chromatin was diluted with TE buffer followed by digestion with 0.2 mg/mL RNase (Life Technologies) and then with 0.2 mg/mL Proteinase K (Life Technologies). DNA was recovered using column purification (ChIP DNA Clean and Concentrator; Zymo). qPCR was performed on precipitated DNA using the following primers: *Klf15* binding site 4, forward 5′-CACCTGTCCCAGTCCAAAGC-3′, reverse 5′-AGGCTGGCTTCAGTTCTTCC-3′; negative control, forward 5′-CATCCAGGAGCCACTGAAAT-3′, reverse 5′-GACATGGACGCTACCTGCTC-3′. Primers amplify the following chromosomal intervals of *Klf15*: SMAD4 binding site (chr6: 90420971–90421737) (76) and PR binding site (chr6: 90420636–90421879) (75) based on mm9. The negative control primer set is for *Fscn2* (chr11:120222708–120222891). Data were normalized to input and expressed as fold enrichment.

Statistical Analysis. Means of the groups were compared by two-tailed Student's *t* test with unequal variance assumed, and differences in the distribution of each group were compared using a two-way ANOVA. Data are presented as mean ± SEM, and $P < 0.05$ was considered statistically significant.

ACKNOWLEDGMENTS. We thank Ruihong Chen and Julio Agno for technical support, Dr. Francesco J. DeMayo and Dr. John P. Lydon for the generous gift of *Pgr-Cre* mice, and Dr. Stephanie Pangas and members of the M.M.M. laboratory for critical comments. These studies were supported by Eunice Kennedy Shriver National Institute of Child Health and Human Development (NICHD) Grants R01-HD033438 and R01-HD032067 and National Institute of General Medical Sciences Grant T32GM008307. The University of Virginia Center for Research in Reproduction Ligand Assay and Analysis Core is supported by the Eunice Kennedy Shriver NICHD/NIH (National Centers for Translational Research in Reproduction and Infertility) Grant P50-HD028934. The content is solely the responsibility of the authors and does not necessarily represent the official views of the National Institutes of Health.

1. Lee KY, Jeong JW, Tsai SY, Lydon JP, DeMayo FJ (2007) Mouse models of implantation. *Trends Endocrinol Metab* 18:234–239.
2. Lee KY, et al. (2007) Bmp2 is critical for the murine uterine decidual response. *Mol Cell Biol* 27:5468–5478.
3. Clementi C, et al. (2013) Activin-like kinase 2 functions in peri-implantation uterine signaling in mice and humans. *PLoS Genet* 9:e1003863.
4. Monsivais D, et al. (2016) Uterine ALK3 is essential during the window of implantation. *Proc Natl Acad Sci USA* 113:E387–E395.
5. Nagashima T, et al. (2013) BMPR2 is required for postimplantation uterine function and pregnancy maintenance. *J Clin Invest* 123:2539–2550.
6. Nakamura T, et al. (1990) Activin-binding protein from rat ovary is follistatin. *Science* 247:836–838.
7. Shimonaka M, Inouye S, Shimasaki S, Ling N (1991) Follistatin binds to both activin and inhibin through the common subunit. *Endocrinology* 128:3313–3315.
8. Thompson TB, Lerch TF, Cook RW, Woodruff TK, Jardetzky TS (2005) The structure of the follistatin:activin complex reveals antagonism of both type I and type II receptor binding. *Dev Cell* 9:535–543.
9. Nakamura T, Sugino K, Titani K, Sugino H (1991) Follistatin, an activin-binding protein, associates with heparan sulfate chains of proteoglycans on follicular granulosa cells. *J Biol Chem* 266:19432–19437.
10. Luisi S, Florio P, Reis FM, Petraglia F (2005) Inhibins in female and male reproductive physiology: Role in gametogenesis, conception, implantation and early pregnancy. *Hum Reprod Update* 11:123–135.
11. Prakash A, Laird S, Tuckerman E, Li TC, Ledger WL (2005) Inhibin A and activin A may be used to predict pregnancy outcome in women with recurrent miscarriage. *Fertil Steril* 83:1758–1763.
12. Prakash A, et al. (2006) A study of luteal phase expression of inhibin, activin, and follistatin subunits in the endometrium of women with recurrent miscarriage. *Fertil Steril* 86:1723–1730.
13. D'Antona D, et al. (2000) Increased maternal serum activin A but not follistatin levels in pregnant women with hypertensive disorders. *J Endocrinol* 165:157–162.
14. Prakash A, et al. (2008) A preliminary study comparing the endometrial expression of inhibin, activin and follistatin in women with a history of implantation failure after IVF treatment and a control group. *BJOG* 115:532–536, discussion 536–537.
15. Matzuk MM, et al. (1995) Multiple defects and perinatal death in mice deficient in follistatin. *Nature* 374:360–363.
16. Guo Q, et al. (1998) Overexpression of mouse follistatin causes reproductive defects in transgenic mice. *Mol Endocrinol* 12:96–106.
17. Jorgez CJ, Klysik M, Jamin SP, Behringer RR, Matzuk MM (2004) Granulosa cell-specific inactivation of follistatin causes female fertility defects. *Mol Endocrinol* 18:953–967.
18. Lin S-Y, et al. (2008) Female infertility and disrupted angiogenesis are actions of specific follistatin isoforms. *Mol Endocrinol* 22:415–429.
19. Kimura F, Sidis Y, Bonomi L, Xia Y, Schneyer A (2010) The follistatin-288 isoform alone is sufficient for survival but not for normal fertility in mice. *Endocrinology* 151: 1310–1319.
20. Holdsworth-Carson SJ, et al. (2015) Follistatin is essential for normal postnatal development and function of mouse oviduct and uterus. *Reprod Fertil Dev* 27:985–999.
21. Craythorn RG, et al. (2012) Progesterone stimulates expression of follistatin splice variants FST288 and FST315 in the mouse uterus. *Reprod Biomed Online* 24:364–374.
22. Candeloro L, Zorn TMT (2007) Distribution and spatiotemporal relationship of activin a and follistatin in mouse decidual and placental tissue. *Am J Reprod Immunol* 58:415–424.
23. Soyal SM, et al. (2005) Cre-mediated recombination in cell lineages that express the progesterone receptor. *Genesis* 41:58–66.
24. Wang H, Dey SK (2006) Roadmap to embryo implantation: Clues from mouse models. *Nat Rev Genet* 7:185–199.
25. Chen Q, et al. (2013) Navigating the site for embryo implantation: Biomechanical and molecular regulation of intrauterine embryo distribution. *Mol Aspects Med* 34: 1024–1042.
26. Hantak AM, Bagchi IC, Bagchi MK (2014) Role of uterine stromal-epithelial crosstalk in embryo implantation. *Int J Dev Biol* 58:139–146.
27. Tong W, Pollard JW (1999) Progesterone inhibits estrogen-induced cyclin D1 and cdk4 nuclear translocation, cyclin E- and cyclin A-cdk2 kinase activation, and cell proliferation in uterine epithelial cells in mice. *Mol Cell Biol* 19:2251–2264.

28. DeSouza MM, et al. (1999) MUC1/episialin: A critical barrier in the female reproductive tract. *J Reprod Immunol* 45:127–158.
29. Thie M, et al. (1995) Cell adhesion to the apical pole of epithelium: A function of cell polarity. *Eur J Cell Biol* 66:180–191.
30. Candia AF, et al. (1997) Cellular interpretation of multiple TGF-beta signals: Intracellular antagonism between activin/BVg1 and BMP-2/4 signaling mediated by Smads. *Development* 124:4467–4480.
31. Ramsdell AF, Yost HJ (1999) Cardiac looping and the vertebrate left-right axis: Antagonism of left-sided Vg1 activity by a right-sided ALK2-dependent BMP pathway. *Development* 126:5195–5205.
32. Yamamoto M, et al. (2009) Antagonism between Smad1 and Smad2 signaling determines the site of distal visceral endoderm formation in the mouse embryo. *J Cell Biol* 184:323–334.
33. Goumans MJ, Lebrin F, Valdimarsdottir G (2003) Controlling the angiogenic switch: A balance between two distinct TGF-b receptor signaling pathways. *Trends Cardiovasc Med* 13:301–307.
34. Rebbapragada A, Benchabane H, Wrana JL, Celeste AJ, Attisano L (2003) Myostatin signals through a transforming growth factor β-like signaling pathway to block adipogenesis. *Mol Cell Biol* 23:7230–7242.
35. Zode GS, Clark AF, Wordinger RJ (2009) Bone morphogenetic protein 4 inhibits TGF-beta2 stimulation of extracellular matrix proteins in optic nerve head cells: Role of gremlin in ECM modulation. *Glia* 57:755–766.
36. Sartori R, et al. (2013) BMP signaling controls muscle mass. *Nat Genet* 45:1309–1318.
37. Winbanks CE, et al. (2013) The bone morphogenetic protein axis is a positive regulator of skeletal muscle mass. *J Cell Biol* 203:345–357.
38. Zhao L, Yee M, O'Reilly MA (2013) Transdifferentiation of alveolar epithelial type II to type I cells is controlled by opposing TGF-β and BMP signaling. *Am J Physiol Lung Cell Mol Physiol* 305:L409–L418.
39. Matzuk MM, Finegold MJ, Su J-GJ, Hsueh AJW, Bradley A (1992) α-inhibin is a tumour-suppressor gene with gonadal specificity in mice. *Nature* 360:313–319.
40. Cipriano SC, Chen L, Kumar TR, Matzuk MM (2000) Follistatin is a modulator of gonadal tumor progression and the activin-induced wasting syndrome in inhibin-deficient mice. *Endocrinology* 141:2319–2327.
41. Li Q, et al. (2007) Prevention of cachexia-like syndrome development and reduction of tumor progression in inhibin-deficient mice following administration of a chimeric activin receptor type II-murine Fc protein. *Mol Hum Reprod* 13:675–683.
42. Li Q, Graff JM, O'Connor AE, Loveland KL, Matzuk MM (2007) SMAD3 regulates gonadal tumorigenesis. *Mol Endocrinol* 21:2472–2486.
43. Pangas SA, et al. (2008) Conditional deletion of Smad1 and Smad5 in somatic cells of male and female gonads leads to metastatic tumor development in mice. *Mol Cell Biol* 28:248–257.
44. Middlebrook BS, Eldin K, Li X, Shivasankaran S, Pangas SA (2009) Smad1-Smad5 ovarian conditional knockout mice develop a disease profile similar to the juvenile form of human granulosa cell tumors. *Endocrinology* 150:5208–5217.
45. Edson MA, et al. (2010) Granulosa cell-expressed BMPR1A and BMPR1B have unique functions in regulating fertility but act redundantly to suppress ovarian tumor development. *Mol Endocrinol* 24:1251–1266.
46. Myers M, Mansouri-Attia N, James R, Peng J, Pangas SA (2013) GDF9 modulates the reproductive and tumor phenotype of female inha-null mice. *Biol Reprod* 88:86.
47. Mansouri-Attia N, et al. (2014) TGFβ signaling promotes juvenile granulosa cell tumorigenesis by suppressing apoptosis. *Mol Endocrinol* 28:1887–1898.
48. Mueller TD, Nickel J (2012) Promiscuity and specificity in BMP receptor activation. *FEBS Lett* 586:1846–1859.
49. Olsen OE, et al. (2015) Activin A inhibits BMP-signaling by binding ACVR2A and ACVR2B. *Cell Commun Signal* 13:27.
50. Aykul S, Martinez-Hackert E (2016) Transforming growth factor-β family ligands can function as antagonists by competing for type II receptor binding. *J Biol Chem* 291: 10792–10804.
51. Lagna G, Hata A, Hemmati-Brivanlou A, Massagué J (1996) Partnership between DPC4 and SMAD proteins in TGF-β signalling pathways. *Nature* 383:832–836.
52. Sidis Y, et al. (2006) Biological activity of follistatin isoforms and follistatin-like-3 is dependent on differential cell surface binding and specificity for activin, myostatin, and bone morphogenetic proteins. *Endocrinology* 147:3586–3597.
53. Park CB, Dufort D (2011) Nodal expression in the uterus of the mouse is regulated by the embryo and correlates with implantation. *Biol Reprod* 84:1103–1110.
54. Park CB, DeMayo FJ, Lydon JP, Dufort D (2012) NODAL in the uterus is necessary for proper placental development and maintenance of pregnancy. *Biol Reprod* 86:194.
55. Gray PC, Harrison CA, Vale W (2003) Cripto forms a complex with activin and type II activin receptors and can block activin signaling. *Proc Natl Acad Sci USA* 100: 5193–5198.
56. Matsuda T, Yamamoto T, Muraguchi A, Saatcioglu F (2001) Cross-talk between transforming growth factor-beta and estrogen receptor signaling through Smad3. *J Biol Chem* 276:42908–42914.
57. Hewitt SC, et al. (2012) Research resource: Whole-genome estrogen receptor α binding in mouse uterine tissue revealed by ChIP-seq. *Mol Endocrinol* 26:887–898.
58. Petraglia F, Florio P, Nappi C, Genazzani AR (1996) Peptide signaling in human placenta and membranes: Autocrine, paracrine, and endocrine mechanisms. *Endocr Rev* 17:156–186.
59. Jones RL, et al. (2002) Expression of activin receptors, follistatin and betaglycan by human endometrial stromal cells; consistent with a role for activins during decidualization. *Mol Hum Reprod* 8:363–374.
60. Florio P, et al. (2003) Endometrial expression and secretion of activin A, but not follistatin, increase in the secretory phase of the menstrual cycle. *J Soc Gynecol Investig* 10:237–243.
61. Jones RL, Salamonsen LA, Findlay JK (2002) Activin A promotes human endometrial stromal cell decidualization in vitro. *J Clin Endocrinol Metab* 87:4001–4004.
62. Tierney EP, Giudice LC (2004) Role of activin A as a mediator of in vitro endometrial stromal cell decidualization via the cyclic adenosine monophosphate pathway. *Fertil Steril* 81:899–903.
63. Tessier C, et al. (2003) Decidual activin: Its role in the apoptotic process and its regulation by prolactin. *Biol Reprod* 68:1687–1694.
64. Gu Y, et al. (1995) Cell-specific expression of activin and its two binding proteins in the rat decidua: Role of alpha 2-macroglobulin and follistatin. *Endocrinology* 136: 3815–3822.
65. Petraglia F, et al. (1994) Local production and action of follistatin in human placenta. *J Clin Endocrinol Metab* 78:205–210.
66. Florio P, et al. (2004) Inhibins and activins in pregnancy. *Mol Cell Endocrinol* 225: 93–100.
67. Jörnvall H, Reissmann E, Andersson O, Mehrkash M, Ibáñez CF (2004) ALK7, a receptor for nodal, is dispensable for embryogenesis and left-right patterning in the mouse. *Mol Cell Biol* 24:9383–9389.
68. Peng J, et al. (2015) Uterine activin-like kinase 4 regulates trophoblast development during mouse placentation. *Mol Endocrinol* 29:1684–1693.
69. Chandra A, Copen CE, Stephen EH (2013) *Infertility and Impaired Fecundity in the United States, 1982-2010: Data from the National Survey of Family Growth* (National Center for Health Statistics, Hayattsville, MD), National Health Statistics Reports, no 67.
70. Sunderam S, et al.; Division of Reproductive Health, National Center for Chronic Disease Prevention and Health Promotion, CDC (2013) Assisted reproductive technology surveillance – United States, 2010. *MMWR Surveill Summ* 67:1–18.
71. Koot YE, Macklon NS (2013) Embryo implantation: Biology, evaluation, and enhancement. *Curr Opin Obstet Gynecol* 25:274–279.
72. National Research Council (2011) *Guide for the Care and Use of Laboratory Animals* (National Academies Press, Washington, DC), 8th Ed.
73. Finn CA, Martin L (1972) Endocrine control of the timing of endometrial sensitivity to a decidual stimulus. *Biol Reprod* 7:82–86.
74. Lee TI, Johnstone SE, Young RA (2006) Chromatin immunoprecipitation and microarray-based analysis of protein location. *Nat Protoc* 1:729–748.
75. Rubel CA, et al. (2012) Research resource: Genome-wide profiling of progesterone receptor binding in the mouse uterus. *Mol Endocrinol* 26:1428–1442.
76. Liu J, et al. (2015) ErbB2 pathway activation upon smad4 loss promotes lung tumor growth and metastasis. *Cell Reports* 10:1599–1613.